LARGE EDDY SIMULATION OF SEPARATION FROM A THREE-DIMENSIONAL HILL AND COMPARISON WITH SECOND-MOMENT-CLOSURE RANS MODELLING

N. Li, C. Wang, A. Avdis and M.A. Leschziner
Department of Aeronautics
South Kensington Campus, Imperial College London,
London SW7 2AZ, United Kingdom
email: n.li@imperial.ac.uk, chen.wang@imperial.ac.uk, mike.leschziner@imperial.ac.uk,
web page:http://www.ae.imperial.ac.uk/tfms/index.html

L. Temmerman
NUMECA International
Av. Franklin Roosevelt, 5
B-1050 Brussels
e-mail: lionel.temmerman@numeca.be

ABSTRACT

LES solutions for the flow separating from a three-dimensional hill in a duct are reported and compared to experiments and second-moment-closure RANS computations. The study was motivated by the observation that even the most elaborate turbulence models, based on non-linear eddy-viscosity formulations and second-moment closure, fail to give a satisfactory representation even of some gross features observed in experiments for the flow at a Reynolds number of 130,000, based on hill height. The comparisons in this study are for the experimental geometry, but at two Reynolds numbers, 13,000 and 130,000, the former enabling better resolution than the latter. Also explored, for the lower Reynolds number, is the sensitivity of the LES solution to the spectral representation of the inflow, found to be substantial. For the lower Reynolds number, the RANS and LES solutions are close. For the real value, however, major differences arise, and the LES solution, on a grid of over 9M cells, also differs greatly from the experimental measurements. In particular, separation is predicted to occur too early, and the extent of the recirculation zone is excessive.

INTRODUCTION

Three-dimensional separation from curved surfaces frequently occurs in external aerodynamics, ship hydrodynamics, turbo-machinery and all manner of curved ducts, curved aero-engine intakes being one example. Unlike separation from a sharp edge, that from a curved surface is always characterised by a highly convoluted and patchy separation area, which moves rapidly in time and space. Separation may also be intermittent and even periodic, associated with von-Karman shedding and/or Taylor-Goertler vortices. Because the separation location is not fixed by a specific geometric feature, its characteristics depend sensitively on the outer flow and also the reattachment process, if occurring at all. In circumstances in which geometric three-dimensionality is relatively weak, a closed recirculation region may arise following separation. This is the case, for example, in a spanwise uniform, unswept cylinder or surface bump which is confined, in the spanwise direction, by walls that are perpendicular to the cylinder or the bump. More generally, the surface of the body interacting with the flow will be highly three-dimensional as is the case with highly-loaded swept wings and fan blades, strongly curved circular ducts and three-dimensional smooth (hill-shaped) constrictions in conduits. In such cases, the separation patterns tend to be much more complex, featuring, in the mean, a wide range of topological entities such as curved detachment and attachment lines and nodes, focal points and saddles (Perry and Chong (1987), Hellman et al. (1990)). Large vortical structures are shed from the surface over a substantial surface area around the mean separation line. Hence turbulence is distinctly non-local, and its dynamics are important. The boundary layer approaching separation is subjected to strong skewing and normal straining, with consequent major changes to the turbulence structure. Finally, strong streamwise vorticity and associated flow curvature within and downstream of the separated region provoke further complex interactions between the mean strain and the turbulence field.

A generic laboratory flow that combines all above features is that around a hill placed in a duct, as shown in Fig. 1. This flow has been examined extensively over several years by Simpson et al. (2002) and Byun & Simpson (2005), using elaborate LDA techniques, and it is increasingly viewed as a key $3D$ test case for prediction procedures. The hill is subjected to a boundary layer of thickness roughly one half of the hill height. The Reynolds number, based on hill height and free-stream velocity, is 130,000. As the boundary layer interacts with the hill, it is subjected to strong skewing prior to separation on the leeward side of the hill. The detached flow evolves as streamwise-oriented vortices bordering a small closed recirculation zone nesting on the hill's leeward side. These vortices lie alongside the legs of a horseshoe vortex formed at the foot of the hill.

Attempts to compute this flow with statistical models have not been successful so far, whether undertaken in steady or unsteady mode, the latter with periodic excitation at inlet. For example, Wang et al. (2004) report a careful study with

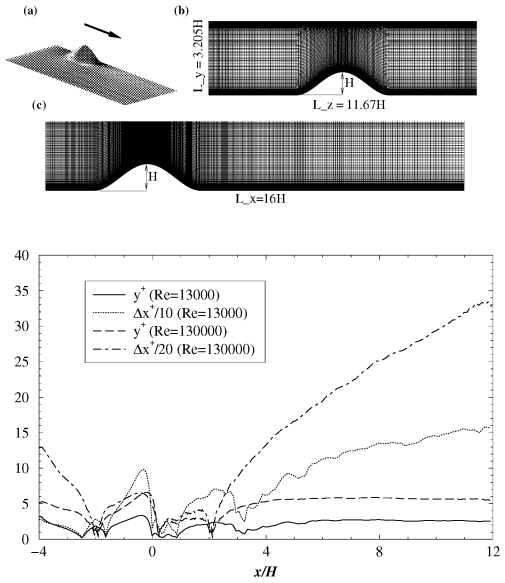

Figure 1: Top: (a) perspective view of the computational domain; (b) grid in y-z plane at $x = 0$; (c) grid in x-y plane at $z = 0$ (b). Bottom: grid characteristics on the centre-plane at hill wall.

various non-linear eddy-viscosity and second-moment-closure models, all giving excessive separation, insufficient rate of post-reattachment recovery and wrong flow topology on the hill surface. These defects are not entirely surprising, as none of the models accounts for the dynamics of the large-scale, highly energetic motions unavoidably accompanying unsteady separation.

A lack of insight into the causes of the major discrepancies noted above has motivated Temmerman et al. (2004) to undertake comparative LES and second-moment-closure computations for the geometry shown in Fig. 1, but for a Reynolds number of 13,000 - that is 10% of the experimental level. The aim of this reduction in Reynolds number was to facilitate an adequate resolution of the near-wall region with a moderately fine grid of 3.5 million nodes. For this relatively low Reynolds number, the LES and the RANS computations returned solutions that were found to be surprisingly close to each other. However, this comparison is subject to considerable uncertainties arising from what is now regarded to be an over-simplified approach to generating the spectral structure of the boundary layer at the computational inlet plane. The present study rectifies this defect and also reports simulations for the experimental Reynolds number of 130,000 in comparison to RANS solutions.

THE COMPUTATIONAL FRAMEWORK

The simulations were performed with a grid containing $192 \times 128 \times 192$ (4.5 million) cells for $Re = 13,000$ and $448 \times 112 \times 192$ (9.2 million) cells for $Re = 130,000$ covering the domain shown in Fig. 1. The lower wall is reasonably well resolved, subject to unavoidable grid-density constraints, while no particular steps were taken to do likewise at the upper or side walls, which are less important. An impression of the grid resolution is conveyed in Fig. 1 by way of distributions of the universal distance of the hill-nearest grid line from the

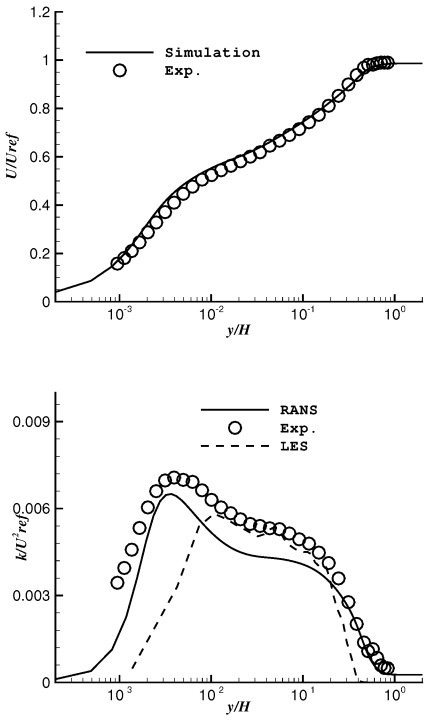

Figure 2: Matching of the mean velocity and turbulent kinetic energy at the inflow plane.

wall in the plane bisecting the hill, and of the streamwise cell length along that same line. As seen, y^+ is of order 2 at the lower Reynolds number, while it rises to order 5 at the higher value. The latter distance is not low enough for a fully-resolved simulation, but a compromise cannot be avoided for this very high Reynolds number in the face of resource constraints.

The inlet conditions are especially important, but posed particular problems, which needed to be addressed with considerable care, even in terms of the mean-flow prescription. Measurements are available only downstream of the hill, and thus no information suitable for prescribing inlet conditions was available in direct form. As reported in detail in Wang et al. (2004), mean-flow conditions were generated computationally by reference to profiles of velocity and Reynolds-stresses measured in the duct, with the hill removed, at the location corresponding to the hill centre-line. Thus, precursor hill-free duct calculations were performed with the RANS method and a non-linear eddy-viscosity model over a length of 20 hills heights. The conditions at the nominal hill-crest position, as returned by the computation, were then determined by carefully matching the computed profiles to the measured duct-flow profiles. This finally allowed conditions 4 hill heights upstream of the hill to be extracted from the hill-free duct computation and prescribed as inlet-velocity condition with the hill present.

The spectral content was generated separately by superposing onto the mean profile fluctuations taken from a separate precursor boundary-layer simulation performed with Lund's quasi-periodic recycling method (Lund (1998)) and rescaling the fluctuations by reference to the ratio of the friction velocity of the simulated boundary layer (at $Re_\theta = 1700$) and

the actual boundary layer ahead of the hill ($Re_\theta = 7000$). As is shown in Fig. 2, the k-profile, evaluated by averaging the rescaled realisation set prescribed at the inlet, only roughly matches the experimental condition. However, it can be argued that having a broadly correct temporal and spatial representation at the inlet plane is far superior to simply securing the statistically correct level of *uncorrelated* fluctuations. At the top and side walls, no special steps are taken to ensure the correct spectral state, as the detailed development of the boundary layers on these walls has an insignificant effect on the main flow features. The outflow was approximated by a non-reflective convective boundary condition.

Subgrid-scale effects are represented by a van-Driest-damped Smagorinsky model with $C_s = 0.1$. This is certainly not the best model that could be used, but it is held to be adequate in the present study, which aims to investigate whether gross flow features can be resolved realistically by LES relative to RANS. Statistical data have been obtained upon integrating the solution over a period corresponding to 40 and 80 times the hill-base diameter for $Re = 13,000$ and $Re = 130,000$, respectively, with the convective speed taken as the unobstructed duct mean-flow velocity. This long integration period is necessitated by the very complex nature of the separation process and the features arising therefrom. An impression of the complexity is conveyed by Fig. 3, which shows a short-time integrated field of the simulated flow. This illustrates the intricate braiding and the large-scale features in the wake of the hill.

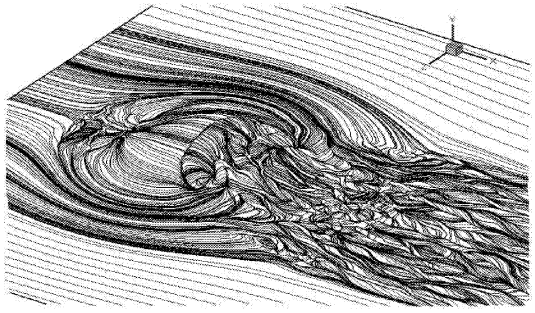

Figure 3: Instantaneous streamlines near the lower surface.

The numerical LES procedure is based on a general non-orthogonal finite-volume approach within which a cell-centred storage and Cartesian velocity decomposition are used. Temporal discretisation is effected by means of a fractional-step method, with the time-derivative being approximated by a second-order backward approximation. The convection and diffusion terms are advanced in time with the Adams-Bashfort method. The pressure is obtained as a solution of the pressure-Poisson problem by means of a $3D$ multigrid algorithm with a SLOR scheme used as smoother. The intermediate cell-centred and contravariant cell-face velocities are then updated via two different representations of the discrete pressure gradient in a manner akin to that proposed by Rhie and Chow (1983). The diffusion terms are discretised using a fully-centred scheme, while the convection scheme uses a blending of a second-order centred scheme and a MUSCL scheme to avoid unphysical numerical oscillations. This is achieved through the implementation of a *wiggle detector* similar to that used by Mary and Sagaut (2001) and Dalshtröm and Davidson (2003). It has been observed that numerical oscillations often occur first in areas where the grid quality is relatively low (normally far away from the regions where important physical processes occur). A closer examination has also shown that less than 2% of the MUSCL scheme is needed in the blending process to avoid unphysical oscillations. This level of upwinding does not affect the physical result. The code is fully parallelised, and the simulations were run on a multi-processor IBM facility.

As regards the RANS results that are included herein, related computational details are provided in Wang et al. (2004) and Temmerman et al. (2004). Briefly, the computations were performed with a non-orthogonal, collocated, cell-centred finite-volume, pressure-based approach over a mesh of 2.2 million nodes, with the near-wall nodal layer located at $y^+ < 1$ throughout. Convection of both mean-flow and turbulence quantities were discretised by a second-order TVD approximation of the QUICK scheme the *UMIST* scheme (Lien and Leschziner (1994)).

RESULTS AND DISCUSSION

In a preliminary study, the importance of the spectral representation of the inflow was investigated by performing two simulations at $Re = 13,000$, one with random noise mimicking inlet turbulence and the other using the realisations derived from the precursor boundary-layer simulation, as described in the previous section. At this much lower Reynolds number, a high level of resolution is much easier to secure, and this is an important consideration when examining the sensitivity to the inflow conditions. All other geometric and flow parameters were identical in the two simulations.

Fig. 4 compares contours of the turbulence energy across the centre-plane obtained from the two simulations, as well as profiles of this energy at one hill height downstream of the hill crest, a location just within the separated zone in both simulations. As seen from the lower contour plot, the random-noise perturbations almost vanish a very short distance downstream of the inlet, a result of the lack of coherence and the violation of the continuity constraint. The turbulence energy only rises at the foot of the hill, due to local separation and strong straining, and then again once separation has occurred beyond the hill crest. On the other hand, the turbulence activity in the near-wall layer is much higher when the precursor realisations are prescribed, and the level is sustained as the flow progresses towards the hill crest. The difference in the turbulent state is conveyed dramatically by the profiles at $x/H = 1.0$, the level of turbulence energy differing by a factor of almost 5. The consequences to the predicted mean-flow features are shown in Fig. 5 in the form of zero-velocity loci in the mid-plane and profile of streamwise velocity at $x/H = 3.0$. The precursor inlet conditions result in a significant upstream shift of the reattachment point on the mid-plane, a less intense wake and a considerably lower strain in the separated shear layer, all consistent with the much higher turbulence level in the flow, especially in the upper shear layer.

The RANS result, derived from the second-moment closure of Shima (1998), is compared in Fig. 6 to the LES, performed with the precursor simulation, by way of topology maps on the hill surface and the lower duct wall. While evidently not identical, the maps indicate that the respective flow fields share some important common features. Thus, separation occurs along similar loci, and the reattachment points on the mid-plate are also close. Finally, the near-wall characteristics in

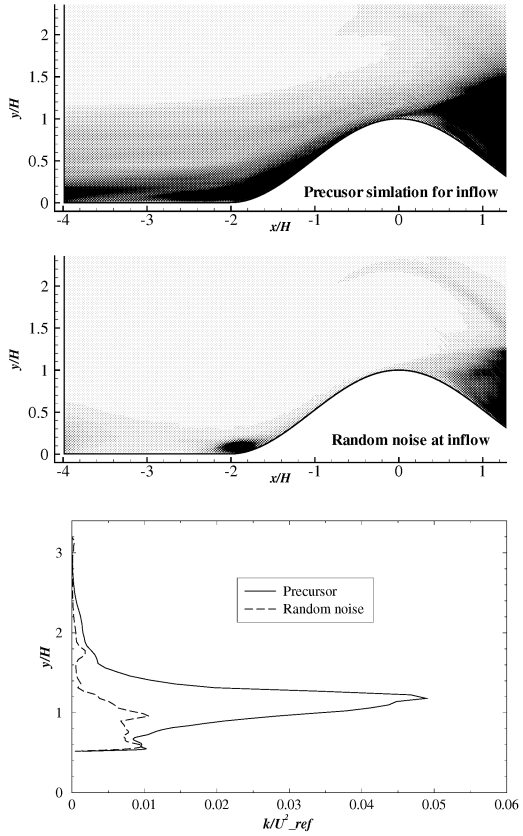

Figure 4: Top: turbulent kinetic energy contour on the centre-plane, with the darkest area $k/U_{ref}^2 > 0.01$; Bottom: k-profiles at $x/H = 1.0$.

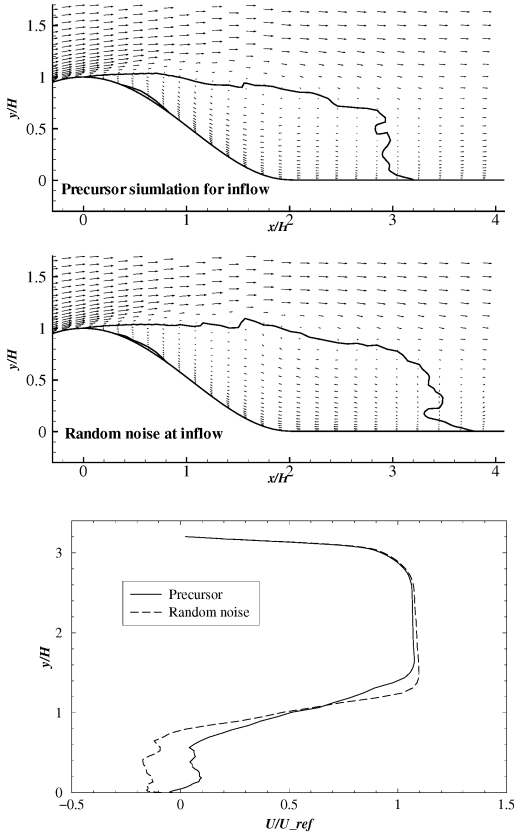

Figure 5: Top: time-averaged velocity vectors on the centre-plane, with the solid line contour of $\overline{U} = 0$; Bottom: velocity profiles at $x/H = 3.0$.

the recovering wake are similar. Hence, this preliminary study shows that the state of the flow upstream of the hill is very influential, and that the second-moment closure used gives a credible representation of the principal features of the flow at the lower Reynolds number. Attention is next directed to the case $Re = 130,000$ corresponding to the actual experimental conditions.

The experimental velocity-field data across the mid-plane, which cannot be reproduced here, show the presence of the small and rather thin recirculation zone on the leeward side of the hill, with separation occurring around $x/H = 0.96$. Furthermore, the flow topology on the hill surface is characterised by a single pair of focal points on either side of the mid-plane, indicating a vortical detachment. Attachment of the flow on the lower wall at the symmetry line occurs very close to the foot of the hill, at $x/H = 2.0$. At this much higher Reynolds number, the LES solution is found to differ substantially from the experimental behaviour, as well as from two RANS solutions obtained, respectively, with the second-moment closure of Speziale et al. (1991) (SSG) and the non-linear eddy-viscosity model (strictly an algebraic second-moment closure) of Abe et al. (2003) (AJL). The most distinctive feature in the LES solution is a seriously premature and sudden separation only a short distance downstream of the hill crest, around $x/H = 0.3$. This is seen both in Fig. 7 and 8. In the latter, showing variations of the pressure coefficient along the centre-line on the hill and duct wall, the LES solution features

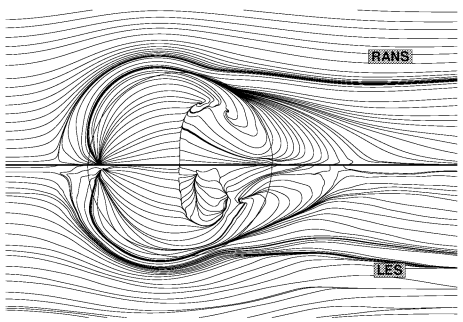

Figure 6: Time-averaged streamlines close to the lower surface. (Re=13,000)

a distinctive kink, followed by a short plateau, which occurs at the location at which the flow suddenly detaches from the hill surface, as identified by the almost straight separation line in Fig. 7. There follows a prolonged recovery at a rate that is much lower than that in the experiment, suggesting the presence of a predominantly two-dimensional, closed and slowly evolving recirculation zone above the mid-portion of the hill, downstream of the separation line. This local 'two-dimensionality' is clearly indicated by the broadly horizontal wall-limiting streamlines downstream of the separation line,

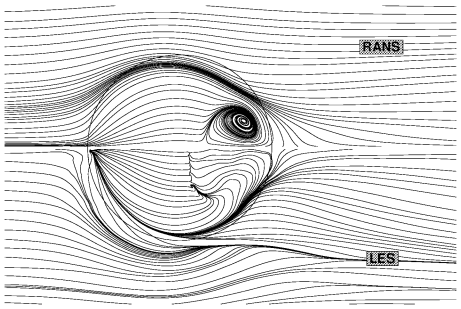

Figure 7: Time-averaged streamlines close to the lower surface. (Re=130,000)

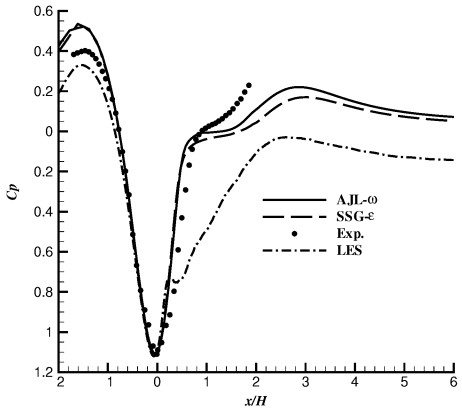

Figure 8: Pressure coefficient on duct centre-plane. (Re=130,000)

around the mid-plane. The absence of a strong lateral motion underneath the recirculation zone, towards the mid-plane, inhibits the recovery from the recirculation and leads to the insufficient rate of increase in pressure. Reattachment on the centre-line occurs at $x/H = 2.0$, which is close to the experiment.

Most measurements available relate to the flow condition in the transverse plane located at $x/H = 3.63$ downstream of the hill crest. For this position, Figs. 9, 10 and 11 show, respectively, skin-friction variations and profiles for velocity and turbulence energy. While the LES-predicted velocity profiles agree reasonably well with the measurements, the turbulence energy is much too high, indicative of the very vigorous turbulence activity associated with the excessive separation. This high level of turbulence, once established upstream of the location considered, leads to a rapid recovery of the wake and thus results, probably fortuitously, in the observed agreement in respect of velocity. Consistent with the predicted high level of turbulence energy is the excessive skin friction seen in Fig. 9.

As noted already, the RANS solutions are very different from that derived from the LES. Other anisotropy-resolving models investigated by Wang et al. (2004) show a qualitatively similar behaviour. With all models, the separation process is much more 'three-dimensional', characterised by a strong vortical footprint in Fig. 7. However, this topological feature (a focus), while also present in the experiment is much too pronounced in the RANS solution. The later separation predicted by the RANS models and the strong lateral motion towards the centre-plane below the vertical separation zone lead to the excessively narrow wake seen in Figs. 7 and 8. Despite the strong lateral motion, reattachment occurs too far downstream, at around $x/H = 2.5$, as indicated by the topology map in Fig. 7. Moreover, post-separation recovery of the pressure, Fig. 8, is too slow, because the turbulence level in the separated shear layer is too low, a characteristic defect displayed by virtually all RANS models.

CONCLUSIONS

The study demonstrates the serious challenges posed by LES when applied to high-Reynolds-number separated flows that are strongly affected by viscous wall processes. While the limitations of RANS have been amply and repeatedly demonstrated for this same type of flow, the predictive capability of LES is not demonstrably superior, albeit for different reasons. For the flow at the higher Reynolds number investigated herein, resolution is clearly a serious problem, and it seems likely that, despite the use of a 9M-node mesh, the solution is affected by numerical errors, to which must be added errors arising from subgrid-scale modelling, because of the relatively coarse mesh used. Insufficient near-wall resolution is the most serious issue. Whether hybrid LES/RANS methods (e.g. Temmerman et al. (2005)) offer a general remedy to this problem remains to be seen. The study has demonstrated that the gross flow features arising from separation from the curved hill surface are materially sensitive to the spectral prescription of the inlet flow. This issue needs to be pursued further – in particular, by using a better precursor for a boundary layer at the requisite (higher) Reynolds number. Given the grid density and the very high computer resources used, the quality of the LES solution for the hill flow is disappointing. While there are major differences between the LES and RANS solutions, the quality of the former, achieved in this study, is poor: separation occurs much too early, the recirculation region is excessive and the turbulence level in the wake is too high, due to the large structures shed by the separation process.

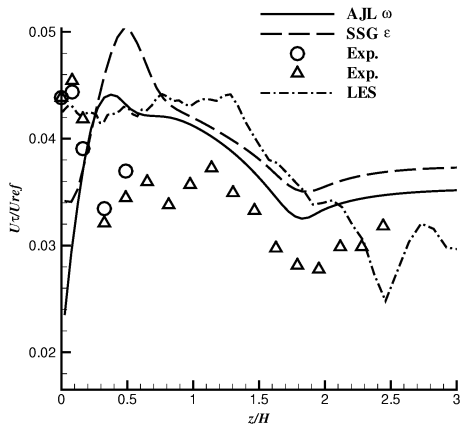

Figure 9: Friction velocity on the lower wall at $x/H = 3.63$. (Re=130,000)

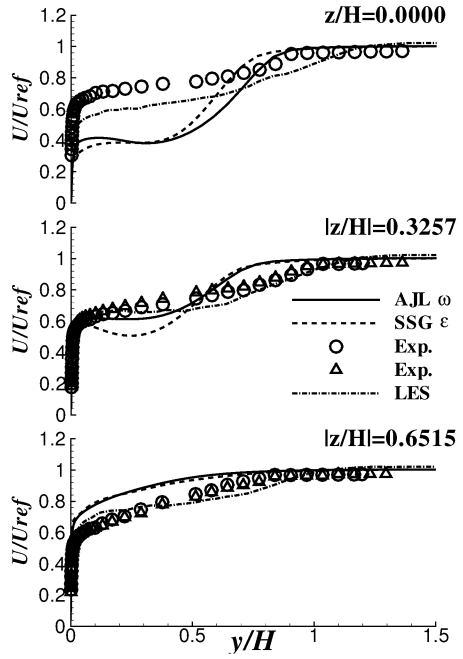

Figure 10: Streamwise velocity at $x/H = 3.63$ and various spanwise z/H locations. (Re=130,000)

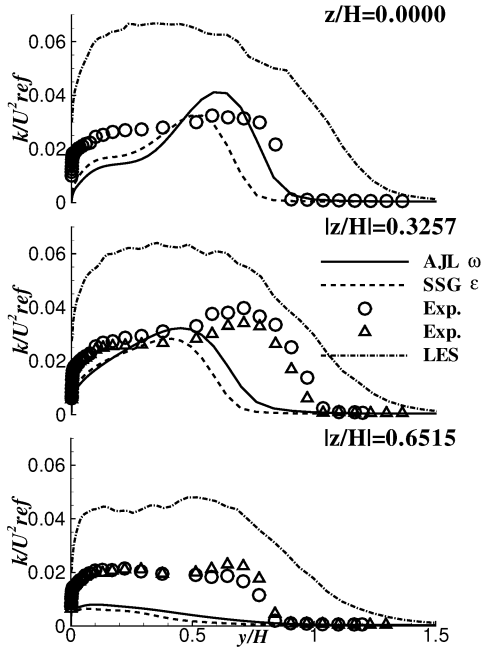

Figure 11: Turbulent kinetic energy at $x/H = 3.63$ and various spanwise z/H locations. (Re=130,000)

ACKNOWLEDGEMENTS

Wang and Leschziner acknowledge the support provided by the EU through the project FLOMANIA (Flow Physics Modelling - An Integrated Approach), a collaboration between Alenia, AEA, Bombardier, Dassault, EADS-CASA, EADS-Military Aircraft, EDF, NUMECA, DLR, FOI, IMFT, ONERA, Chalmers University, Imperial College London, TU Berlin, UMIST and St. Petersburg State University. The project is funded by the European Union and administrated by the CEC, Research Directorate-General, Growth Programme, under Contract No. G4RD-CT2001-00613.

Li, Temmerman, Avdis and Leschziner are grateful to EPSRC for their financial support and the provision of computing resources on the Origin 3000 machine through the CSAR national centre in Manchester.

REFERENCES

Abe, K., Jang, Y.J., and Leschziner, M.A., 2003 "An investigation of wall-anisotropy expressions and length-scale equations for non-linear eddy-viscosity models". *Int. J. Heat Fluid Flow*, **24**, 181–198.

Byun, G., and Simpson, R.L., 2005 "Structure of three-dimensional separated flow on an axisymmetric bump". AIAA Paper 2005-0113.

Dahlström, S., and Davidson, L., 2003 "Large eddy simulation applied to a high-Reynolds flow around an airfoil close to stall". AIAA Paper 2003-0776.

Helman, J.L., and Hesselink, L., 1990 "Surface representations of two- and three-dimensional fluid flow topology". *Proceedings of the 1st conference on Visualization '90*, 6–13.

Lien, F.S., and Leschziner, M.A., 1994 "A general non-orthogonal collocated finite volume algorithm for turbulent flow at all speeds incorporating second-moment turbulence-transport closure. Part 1: Computational implementation." *Comput. Methods Appl. Mech. Engrg*, **114**, 123–148.

Lund, T.S., Wu, X. and Squires, K.D., 1998 "Generation of turbulent inflow data for spatially-developing boundary layer simulations". *J. Comp. Phys.*, **140** (2), 233–258.

Mary I., and Sagaut P., 2001 "Large eddy simulation of flow around an airfoil near stall". *AIAA J.*, **40** (6), 1139–1145.

Perry, A.E., and Chong, M.S., 1987 "A description of eddying motions and flow patterns using critical-point concepts". *Ann. Rev. Fluid Mech.*, **19**, 125–155.

Rhie, C.M., and Chow, W.L., 1983 "Numerical study of the turbulent flow past an airfoil with trailing edge separation". *AIAA J.*, **21** (11), 1525–1532.

Shima, N., 1998 "Low-Reynolds-number second-moment closure without wall-reflection redistribution terms". *Int. J. Heat and Fluid Flow*, **19**, 549–555.

Simpson, R.L., Long, C.H., and Byun, G., 2002 "Study of vortical separation from an axisymmetric hill". *Int. J. Heat and Fluid Flow*, **23**, 582–591.

Speziale, C.G., Sarkar, S., and Gatski, T.B., 1991 "Modelling the pressure-strain correlation of turbulence: an invariant dynamical systems approach". *J. Fluid Mech.* **227**, 245–272.

Temmerman, L., Hadžiabdić, M., Leschziner, M.A., and Hanjalić, K., 2005 "A hybrid two-layer URANS-LES approach for large eddy simulation at high Reynolds numbers". *Int. J. Heat and Fluid Flow*, **26**, 173–190.

Temmerman, L., Wang, C., and Leschziner, M.A., 2004 "A comparative study of separation from a three-dimensional hill using larger eddy simulation and second-moment-closure RANS modelling". *4th European Congress on Computational Methods in Applied Sciences and Engineering, ECCOMAS.*

Wang, C., Jang, Y.J., and Leschziner, M.A., 2004 "Modelling two and three-dimensional separation from curved surfaces with anisotropy-resolving turbulence closures". *Int. J. Heat and Fluid Flow*, **25**, 499–512.